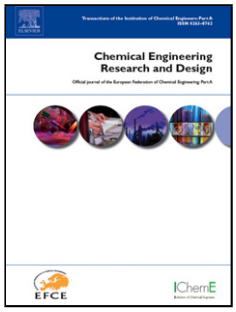

Title: Mathematical Modelling of the Evolution of the Particle Size Distribution during Ultrasound-Induced Breakage of Aspirin Crystals

Authors: Michael L. Rasche, Brad W. Zeiger, Kenneth S. Suslick, Richard D. Braatz

PII: S0263-8762(18)30016-9
DOI: https://doi.org/10.1016/j.cherd.2018.01.014
Reference: CHERD 2988

To appear in:

Received date: 24-4-2015
Revised date: 5-12-2017
Accepted date: 6-1-2018

Please cite this article as: Rasche, Michael L., Zeiger, Brad W., Suslick, Kenneth S., Braatz, Richard D., Mathematical Modelling of the Evolution of the Particle Size Distribution during Ultrasound-Induced Breakage of Aspirin Crystals.Chemical Engineering Research and Design https://doi.org/10.1016/j.cherd.2018.01.014

Mathematical Modelling of the Evolution of the Particle Size Distribution during Ultrasound-Induced Breakage of Aspirin Crystals

Michael L. Rasche,[a] Brad W. Zeiger,[b] Kenneth S. Suslick,[b] and Richard D. Braatz[a,c]

[a] Dept. of Chemical & Biomolecular Engineering, University of Illinois, Urbana-Champaign, IL
[b] Dept. of Chemistry, University of Illinois, Urbana-Champaign, IL
[c] Massachusetts Institute of Technology, 77 Massachusetts Avenue, Room 66-372, Cambridge, MA (braatz@mit.edu)

Highlights

- A mathematical model is derived for the crystal breakage that results from ultrasound
- Population balance models are developed for three models of binary breakage events
- Dependencies of cavitation rate on applied power and solvent viscosity are provided
- Agreement with experiments is good for aspirin crystals undergoing sonofragmentation
- Analysis supports the model in which crystals break into two equal-sized particles

Abstract

While the effects of ultrasound on crystals have been heavily investigated experimentally, population balance models that describe the effects of all physical parameters such as solution viscosity and applied power on the crystal size distribution have been lacking. This article presents one of the first population balance models for describing the crystal breakage that results from ultrasound. Aspirin crystals dispersed in various solvents, dodecane and silicon oils of known viscosity, were subjected to ultrasound to study this sonofragmentation that occurs due to cavitation when bubbles violently collapse, creating extreme conditions in the immediate vicinity of the bubbles. Population balance models are developed with three models for binary breakage events and cavitation rate proportional to the applied power and exponentially related to solvent viscosity. The resulting population balance models provide reasonable agreement with the experimental data over the ranges of applied power and solvent viscosity investigated, with nearly overlapping crystal size distributions for applied power between 10 and 40 W. The statistical analysis supports the breakage model in which cavitation bubbles cause the aspirin crystals to break into two equal-sized particles.

Keywords: ultrasound; population balance modeling, crystallization; particle technology; kinetics estimation

1 Introduction

The application of high-intensity ultrasound to crystallization is an area of significant interest and is as an effective technique for inducing nucleation and controlling particle size distributions. While the effects of ultrasound on crystals have seen some experimental investigation (Devarakonda et al., 2004; Guo et al., 2007; Raman et al., 2008; Wagterveld et al., 2011; Teipel et al., 2002; 2004), population balance models that describe the effects of all physical parameters such as liquid viscosity and applied power on the crystal size distribution have been lacking. Raman et al. (2011) demonstrated the application of Kapur function analysis to obtain grinding kinetics in a system of inorganic particles dispersed in water. This paper presents a different approach to modeling ultrasonic breakage for an organic system over a range of shorter times and lower ultrasound intensity and specifically investigates the effect of varying solvent viscosity.

Aspirin crystals dispersed in the nonsolvent dodecane were subjected to ultrasound to study this *sonofragmentation*, which occurs due to acoustic cavitation, which is the formation, growth, and implosive collapse of bubbles in an ultrasonic field. The final bubble collapse results in extreme local temperatures and pressures and produces high-pressure shockwaves that propagate through the liquid (Doktycz & Suslick, 1990; Suslick et al., 1999). The time evolution of the crystal size distribution is described by the population balance equation for breakage only with three models for binary breakage events: (A) crystals break in half; (B) crystals break with uniform probability into each pair of sizes allowed by the discretization of the length axis; and (C) crystals break with nonuniform probability into each pair of sizes allowed by the discretization of length. Models A and B have two parameters that describe the breakage rate as a function of applied power and solvent viscosity, while Model C also includes a third parameter that is the standard deviation σ of the breakage distribution.

The remainder of this paper is organized as follows. A description of the methodology and mathematical model is followed by a comparison and discussion of the simulation results.

2 Materials and Methods

2.1 Population Balance Models

The experimental setup for the sonofragmentation experiments is shown in Fig. 1 and described by Zeiger & Suslick (2011). Nonsolvents dodecane (viscosity = 1.8 cSt) and silicone oil (viscosity = 20, 50, 100, 115, 154, 220, 244, 350, 500, and 1000 cSt) are used to disperse the

crystals. Various power levels (3, 5, 10, 20, 30, 40 W) are applied to the ultrasound horn for 1 minute, which caused cavitation and crystal breakage.

Crystals are characterized in terms of circularity and surface area as measured via optical microscopy. The circularity is defined as

$$c = \frac{4\pi a}{p^2} \tag{1}$$

where a is the surface area and p is the perimeter of the two-dimensional image of the crystal (see Fig. 1c). The crystal depth d, defined as the shortest dimension, is estimated from the surface area and perimeter using a proportionality constant obtained from the scanning electron microscope (SEM) images assuming that the particles have a similar shape:

$$d \approx \frac{a}{2.06\,p}. \tag{2}$$

The mass for each particle was calculated from

$$m = \rho a d \tag{3}$$

where ρ is the crystal density.

The sonofragmentation was modeled by the population balance equation for breakage only (Tan et al., 2004),

$$\frac{\partial}{\partial t}[n(t,m)] = \int_m^\infty S(u)b(m,u)n(t,u)du - S(m)n(t,m), \tag{4}$$

where S is the breakage rate, b is the breakage function, n is the number density function, and m is the crystal mass. The breakage rate S [1/s] in (4) is assumed to follow the standard power-law function of the crystal mass (Tan et al., 2004):

$$S(m) = S_1 m^q, \qquad q \geq 0, \tag{5}$$

with exponent q and selection rate constant S_1 related to the cavitation rate. For any $q > 0$, this expression has the breakage rate approaching zero as the crystal mass m approaches zero. In any single experiment, the average breakage rate per particle would reduce over time and further reduction in the number density function would become slower over time until appearing to approach a limiting value over the finite time duration of the single experiment.

The cavitation rate has been reported to be proportional to the applied power over the ranges considered here (Colussi et al., 1999; Son et al., 2009). Experimentally, the cavitation rate was

observed to be exponentially related to the liquid viscosity η (in cSt, see Fig. 2). Combining these relationships provides an expression for S_1:

$$S_1 = S_0 \Pi \exp(-0.0069\eta), \tag{6}$$

where the applied power Π is in units of Watts. This model does not consider dependencies on additional parameters such as surface tension or equilibrium vapor pressure of the liquid.

2.2 Breakage Models

Here a procedure is described for simulation of the population balance equation for breakage (1). This matrix approach is similar to that developed for coal milling processes (Broadbent et al., 1956). The minimum crystal mass that can occur during the breakage experiments, $m_{\min}$, was chosen and the crystal mass data scaled by a constant so that $m_{\min} = 1$. The discretization of the crystal mass m was selected so that $\Delta m = m_{\min} = 1$, which results in all scaled crystal masses taking on integer values (e.g., see Fig. 3). Assuming that crystals break into two crystals of equal mass for even integer masses and nearly equal masses for odd integer masses (e.g., a crystal with mass of 4 breaks into two crystals of mass 2; a crystal with mass of 5 breaks into two crystals of masses 2 and 3), the breakage function b in (1) can be written as

$$b(m,u) = \begin{cases} 2, & u = 2m \\ 1, & u = 2m+1 \\ 1, & u = 2m-1 \\ 0, & \text{otherwise} \end{cases} \tag{7}$$

Discretizing the population balance equation (1) with respect to mass results in

$$\frac{\partial}{\partial t}[n(t,m_i)] = \begin{cases} 2S_1(2m_i)^q n(t,2m_i) + S_1(2m_i+1)^q n(t,2m_i+1), & i = 1 \\ 2S_1(2m_i)^q n(t,2m_i) + S_1(2m_i+1)^q n(t,2m_i+1) + S_1(2m_i-1)^q n(t,2m_i-1) - S_1(m_i)^q n(t,m_i), & i = 1 < i < i_{\max}/2 \\ 2S_1(2m_i)^q n(t,2m_i) + S_1(2m_i-1)^q n(t,2m_i-1) - S_1(m_i)^q n(t,m_i), & i = i_{\max}/2 \\ -S_1(m_i)^q n(t,m_i), & i_{\max}/2 < i \le i_{\max} \end{cases} \tag{8}$$

where $i_{\max}$ is defined by the largest crystal size. The time derivative is replaced with the first-order forward-difference approximation,

$$\frac{\partial}{\partial t}[n(t,m_i)] \approx \frac{n(t_{j+1},m_i) - n(t_j,m_i)}{\Delta t}, \tag{9}$$

with the initial condition determined by the mass distribution of unbroken crystals CSD that was experimentally measured (Figs. 4 & S1). To prevent negative values for n from occurring due to discretization error for very high values of S_0 and q in (4)–(5), the timestep was set to satisfy

$$\Delta t \le \frac{1}{4S_1 m_{\max}^q}. \tag{10}$$

The right-hand side of (4) was written as the multiplication of a vector and a sparse matrix:

$$n(t_{j+1}) = n(t_j)A \tag{11}$$

where $n(t_j)$ is a row vector of length $i_{\max}$ and A is a lower diagonal square matrix with an interesting structure, with the 10×10 case being

$$A = \begin{bmatrix} 1 & 0 & 0 & 0 & 0 & 0 & 0 & 0 & 0 & 0 \\ 2\beta_2 & 1-\beta_2 & 0 & 0 & 0 & 0 & 0 & 0 & 0 & 0 \\ \beta_3 & \beta_3 & 1-\beta_3 & 0 & 0 & 0 & 0 & 0 & 0 & 0 \\ 0 & 2\beta_4 & 0 & 1-\beta_4 & 0 & 0 & 0 & 0 & 0 & 0 \\ 0 & \beta_5 & \beta_5 & 0 & 1-\beta_5 & 0 & 0 & 0 & 0 & 0 \\ 0 & 0 & 2\beta_6 & 0 & 0 & 1-\beta_6 & 0 & 0 & 0 & 0 \\ 0 & 0 & \beta_7 & \beta_7 & 0 & 0 & 1-\beta_7 & 0 & 0 & 0 \\ 0 & 0 & 0 & 2\beta_8 & 0 & 0 & 0 & 1-\beta_8 & 0 & 0 \\ 0 & 0 & 0 & \beta_9 & \beta_9 & 0 & 0 & 0 & 1-\beta_9 & 0 \\ 0 & 0 & 0 & 0 & 2\beta_{10} & 0 & 0 & 0 & 0 & 1-\beta_{10} \end{bmatrix} \tag{12}$$

with the coefficients β_i specified by (8). The matrix A consists of entries along the main diagonal and a band of 3 entries wide centered in the lower diagonal part of A. Explicitly defining the matrix as sparse in MATLAB speeds computations and decreases the memory requirement.

An alternative breakage model has each crystal breaking into two crystals according to a uniform distribution (by number) of each crystal mass smaller than the parent crystal. The matrix analogous to A for the 10×10 case is

$$B=\begin{bmatrix}
1 & 0 & 0 & 0 & 0 & 0 & 0 & 0 & 0 & 0 \\
2\alpha_2\beta_2 & 1-\beta_2 & 0 & 0 & 0 & 0 & 0 & 0 & 0 & 0 \\
\alpha_3\beta_3 & \alpha_3\beta_3 & 1-\beta_3 & 0 & 0 & 0 & 0 & 0 & 0 & 0 \\
\alpha_4\beta_4 & 2\alpha_4\beta_4 & \alpha_4\beta_4 & 1-\beta_4 & 0 & 0 & 0 & 0 & 0 & 0 \\
\alpha_5\beta_5 & \alpha_5\beta_5 & \alpha_5\beta_5 & \alpha_5\beta_5 & 1-\beta_5 & 0 & 0 & 0 & 0 & 0 \\
\alpha_6\beta_6 & \alpha_6\beta_6 & 2\alpha_6\beta_6 & \alpha_6\beta_6 & \alpha_6\beta_6 & 1-\beta_6 & 0 & 0 & 0 & 0 \\
\alpha_7\beta_7 & \alpha_7\beta_7 & \alpha_7\beta_7 & \alpha_7\beta_7 & \alpha_7\beta_7 & \alpha_7\beta_7 & 1-\beta_7 & 0 & 0 & 0 \\
\alpha_8\beta_8 & \alpha_8\beta_8 & \alpha_8\beta_8 & 2\alpha_8\beta_8 & \alpha_8\beta_8 & \alpha_8\beta_8 & \alpha_8\beta_8 & 1-\beta_8 & 0 & 0 \\
\alpha_9\beta_9 & \alpha_9\beta_9 & \alpha_9\beta_9 & \alpha_9\beta_9 & \alpha_9\beta_9 & \alpha_9\beta_9 & \alpha_9\beta_9 & \alpha_9\beta_9 & 1-\beta_9 & 0 \\
\alpha_{10}\beta_{10} & \alpha_{10}\beta_{10} & \alpha_{10}\beta_{10} & \alpha_{10}\beta_{10} & 2\alpha_{10}\beta_{10} & \alpha_{10}\beta_{10} & \alpha_{10}\beta_{10} & \alpha_{10}\beta_{10} & \alpha_{10}\beta_{10} & 1-\beta_{10}
\end{bmatrix} \tag{13}$$

with the values β_i being the same as defined above. Assuming each integer breakage is equally probable, the parameter

$$\alpha_i=\begin{cases}\dfrac{2}{i-1}, & i \text{ odd} \\ \dfrac{2}{i}, & i \text{ even}\end{cases} \tag{14}$$

ensures an overall conservation of mass. A third alternative model assumes that the particles resulting from breakage are normally distributed, which for the 10×10 case replaces the matrix A by

$$C=\begin{bmatrix}
1 & 0 & 0 & 0 & 0 & 0 & 0 & 0 & 0 & 0 \\
2\alpha_{2,1}\beta_2 & 1-\beta_2 & 0 & 0 & 0 & 0 & 0 & 0 & 0 & 0 \\
\alpha_{3,1}\beta_3 & \alpha_{3,2}\beta_3 & 1-\beta_3 & 0 & 0 & 0 & 0 & 0 & 0 & 0 \\
\alpha_{4,1}\beta_4 & 2\alpha_{4,2}\beta_4 & \alpha_{4,3}\beta_4 & 1-\beta_4 & 0 & 0 & 0 & 0 & 0 & 0 \\
\alpha_{5,1}\beta_5 & \alpha_{5,2}\beta_5 & \alpha_{5,3}\beta_5 & \alpha_{5,4}\beta_5 & 1-\beta_5 & 0 & 0 & 0 & 0 & 0 \\
\alpha_{6,1}\beta_6 & \alpha_{6,2}\beta_6 & 2\alpha_{6,3}\beta_6 & \alpha_{6,4}\beta_6 & \alpha_{6,5}\beta_6 & 1-\beta_6 & 0 & 0 & 0 & 0 \\
\alpha_{7,1}\beta_7 & \alpha_{7,2}\beta_7 & \alpha_{7,3}\beta_7 & \alpha_{7,4}\beta_7 & \alpha_{7,5}\beta_7 & \alpha_{7,6}\beta_7 & 1-\beta_7 & 0 & 0 & 0 \\
\alpha_{8,1}\beta_8 & \alpha_{8,2}\beta_8 & \alpha_{8,3}\beta_8 & 2\alpha_{8,4}\beta_8 & \alpha_{8,5}\beta_8 & \alpha_{8,6}\beta_8 & \alpha_{8,7}\beta_8 & 1-\beta_8 & 0 & 0 \\
\alpha_{9,1}\beta_9 & \alpha_{9,2}\beta_9 & \alpha_{9,3}\beta_9 & \alpha_{9,4}\beta_9 & \alpha_{9,5}\beta_9 & \alpha_{9,6}\beta_9 & \alpha_{9,7}\beta_9 & \alpha_{9,8}\beta_9 & 1-\beta_9 & 0 \\
\alpha_{10,1}\beta_{10} & \alpha_{10,2}\beta_{10} & \alpha_{10,3}\beta_{10} & \alpha_{10,4}\beta_{10} & 2\alpha_{10,5}\beta_{10} & \alpha_{10,6}\beta_{10} & \alpha_{10,7}\beta_{10} & \alpha_{10,8}\beta_{10} & \alpha_{10,9}\beta_{10} & 1-\beta_{10}
\end{bmatrix} \tag{15}$$

where

$$\alpha_{i,j} = \begin{cases} \dfrac{1}{\sigma\sqrt{2\pi}} \exp\left[-\dfrac{i-2j}{4\sigma^2} \right], & j \le i \\ \alpha_{i,i_{\max}-j}, & j > i \end{cases} \tag{16}$$

and σ is the standard deviation of the normal distribution. Mass is conserved by rescaling the values of $\alpha_{i,j}$ in (16) so that $\sum_j j\alpha_{i,j} = i$ for odd *i*, and $\sum_j j\alpha_{i,j} + j\alpha_{i,j/2} = i$ for even *i*. This model has the highest probability that crystals break into equal sizes, with monotonically lower probability as the difference in size between the broken crystals become larger. Since the curve is symmetric, in row 10, $\alpha_{10,5}$ is the maximum value and $\alpha_{10,4} = \alpha_{10,6}$, etc.

2.3 Parameter Estimation

Each model produces a mass distribution for specified values of the two model parameters, S_0 and q, which were compared to the experimental data by comparing cumulative mass distributions F_{model} and F_{exp}. The use of cumulative distributions avoids the binning errors that arise when histograms are used to approximate distributions. Under the assumption of additive independent measurement errors, the maximum-likelihood and minimum-variance parameters based on the Riemann-sum approximation of the integral-form for the squared error are the solution of the optimization

$$\min_{\underline{\theta}} \sum_i \sum_j \frac{1}{\sigma_{ij}^2} \left[F_{\text{model}}(t_j, m_i; \underline{\theta}) - F_{\text{exp}}(t_j, m_i) \right]^2 \Delta t_j \, \Delta m_i \tag{17}$$

With the assumption that the σ_{ij} are all equal, the Δt_j are all equal and setting $\Delta m_i = 1$ weighs the cumulative mass distributions more heavily where more data points have been collected; with *E* equal to the difference between the model and experimental cumulative distributions, the expression (17) can be simplified to

$$R = \min_{\underline{\theta}} \sum_i \sum_j E_{ij}^2 = \min_{\underline{\theta}} \sum_i \sum_j \left(E^{\mathrm{T}} E \right)_{ij} \tag{18}$$

MATLAB is inherently slow when dealing with loops and fast when using matrix-vector arithmetic. Objective (17) can be computed as a single function call to the Frobenius norm of the matrix *E*, or the elements of the matrix *E* can be stacked as a long vector and the objective computed using the vector 2-norm or vector-vector multiply commands.

Confidence regions for the parameters $\underline{\theta} = [S_0 \; q]^{\mathrm{T}}$ were estimated using the *F* distribution (Beck & Arnold, 1977),

$$\frac{S(\underline{\theta})-R}{R/(n-p)} \approx F_{1-\alpha}(p, n-p), \tag{19}$$

where the sum-of-squared-deviations $S(\underline{\theta})$ is the objective function in (18), n is the number of data points, p is the number of parameters, and $1-\alpha$ is the confidence level for the region.

3 Results and Discussion

The parameters for the model that assumes equal-size binary breakage were estimated from the experimental data from 1-minute trials for aspirin in dodecane for 6 different levels of ultrasonic power. The confidence regions around the maximum-likelihood estimates of the efficiency factor $S_{0,\text{opt}} = 9.8\times10^{-4}$ and $q_{\text{opt}} = 0.074$ are shown in Fig. S2. The uncertainties in the efficiency factor S_0 are <10% but somewhat larger for the exponent q on a relative basis. The positive value for exponent q indicates that large crystals are more likely to break than small particles, but that the dependency is rather small. The crystal size distribution for the population balance model for crystal breakage in the presence of ultrasound nearly overlaps the experimental data for applied power between 10 and 40 W, with noticeable deviations for 3 and 5 W (see Fig. 5). A potential explanation is that the linear dependency on applied power in Eq. 6 is less accurate at low values of applied power. The population balance model quantitatively described the changes in the mass distributions due to increased breakage as ultrasonic intensity increased (Fig. 5).

A second set of experiments measured the effects on ultrasound on the cumulative mass distributions for aspirin in silicone oils of 10 different viscosities (see Fig. 6). As before, the cumulative mass distributions obtained for the best-fit model parameters were in agreement with experimental data. The model quantitatively described the effect of decreased breakage on the mass distributions as the liquid viscosity increases, due to decreased cavitation (for increased liquid viscosity, more energy would be required to induce cavitation). The confidence regions computed for the best-fit model parameters $S_{0,\text{opt}} = 8.8\times10^{-4}$ and $q_{\text{opt}} = 5.6\times10^{-6}$ are shown in Fig. S3, which show less than 2% uncertainty in the efficiency factor S_0. For this set of experiments, the value of zero for the exponent q falls within the confidence regions indicating that the dependency of the breakage rate on mass was not statistically significant for silicone oils with this range of viscosities. One possible explanation for this observation is that larger crystals interact with more cavitation bubbles per unit time but have more inertia are so are less affected

by each cavitation bubble, and these competing effects cancel so that the effect of the mass on the breakage rate is negligible. In either case, it is encouraging that the values of the two best-fit model parameters are similar for the varying ultrasonic power and varying viscosity data sets.

For the uniform breakage model (13), the best-fit model parameters were $S_{0,opt} = 8.3\times10^{-6}$ and $q_{opt} = 1.1$ for the experiments with varying ultrasonic power and $S_{0,opt} = 2.6\times10^{-8}$ and $q_{opt} = 2.0$ for the experiments with varying liquid viscosity. The corresponding confidence regions for the model parameters are shown in Figs. S4–S5, which show 10 to 20% uncertainty in S_0. An interesting observation from Figs. S4–S5 for the uniform binary breakage model is that the best-fit exponent q_{opt} has nominal values that are very close to integers with very small confidence intervals. The uncertainties in the efficiency factor S_0 are much larger and the fits to the experimental cumulative mass distributions for the uniform breakage model in Figs. S6–S7 are not as good as for the equal-size breakage model, as shown by comparing coefficients of determination in Table 1. Further, the values for the two best-fit parameters are very different for the varying ultrasonic power and varying viscosity data sets. As such, it is not recommended to try to read too much meaning into the best-fit exponent q_{opt} having nearly integer values.

The reduction in fitting capability observed in the uniform breakage model motivated the third breakage model (15) that includes an additional parameter, which is a standard deviation. In comparison to the 2-parameter models, a high value for the standard deviation approximates the uniform breakage model, while a standard deviation approaching zero is asymptotic to the equal-size breakage model. The best-fit model parameters were $S_{0,opt} = 7.1\times10^{-4}$, $q_{opt} = 0.16$, and $\sigma_{opt} = 32$ for the experiments with varying ultrasonic power and $S_{0,opt} = 8.8\times10^{-4}$, $q_{opt} = 1.3\times10^{-13}$, and $\sigma_{opt} = 0.12$ for the experiments with varying liquid viscosity. A value of $\sigma_{opt} = 32$ corresponds to a broad size range for broken particles whereas $\sigma_{opt} = 0.12$ corresponds very closely to the equal-size breakage model. The values for the best-fit model parameters $S_{0,opt} = 8.8\times10^{-4}$ and $q_{opt} \approx 0$ for the varying liquid viscosity experiments for the three-parameter model are statistically indistinguishable from values obtained by the equal-size breakage model (Table 1). For both data sets, the 3-parameter breakage model does not provide a significant improvement in fit to the experimental data (e.g., cf Figs. 5 and 6 with Figs. S8–S9). Confidence regions for the 3-parameter model (15) are shown in Figs. S10–S11 as projections onto 2D planes for power and viscosity, respectively. The relative uncertainties in the model parameters q and σ are large for

the experiments with varying viscosity (Fig. S11) and the best-fit values for both parameters are near zero, providing further lack of experimental support for the three-parameter model.

The above statistical analysis supports the equal-size breakage model. Additional support is provided by close inspection of the experimental cumulative mass distributions for the varying liquid viscosity. For the highest values of the viscosity (e.g., ≥ 220 cSt), the particle size distribution (Fig. 6) is nearly indistinguishable the initial size distribution (Fig. S1), with more than 5% of the crystals with mass of 11–14 ng (1.1×10^{-11}–1.4×10^{-11} kg). At the high liquid viscosity, cavitation bubbles have insufficient energy to break the particles. As the viscosity is reduced from 220 to 100 cSt, the number of particles around 11–14 ng (1.1×10^{-11}–1.4×10^{-11} kg) monotonically decreases, without observing any crystals between 7 ng and the group of particles at 11–14 ng (1.1×10^{-11}–1.4×10^{-11} kg). If the particles broke into two equal-sized pieces, then the particles of mass 11–14 ng would break to produce crystals of 5.5–7 ng (5.5×10^{-12}–7×10^{-12} kg), which would all be less than 7 ng (7×10^{-12} kg) just as seen in Fig. 6. If the particles broke into multiple particles of other sizes, then particles would be observed between 7 and 11 ng (7×10^{-12}–1.1×10^{-11} kg). The experimental data support both the assumptions that the particles break into two particles and the two particles are equal sizes, that is, the binary equal-size breakage model. Further, the breakage rate in this model was well described by combining (5) and (6) and setting $q = 0$ to give

$$S(m) = S_0 \Pi \exp(-0.0069\eta), \tag{20}$$

which is proportional to the ultrasonic power, exponentially decreasing with respect to the liquid viscosity, and independent of the particle mass.

The breakage of particles into equal-sized particles has not been observed in some other systems, such as Al_2O_3 particles (Raman and Abbas, 2008). One question that arises is why the statistical analysis indicates that each aspirin crystal breaks into two crystals of equal mass. This observation is likely to be associated with the particle shape of the aspirin crystals, which were thin and flat (Fig. 1c). The torque on the crystals is largest along the longest of the three directions and so each crystal is most likely to break along the longest direction in response to the force generated by imploding cavitation bubbles. Similarly, the minimum torque required to break a flat thin crystal in half is lower than the torque required to break the crystal in any other location.

The population balance model was also compared to particle size data collected for experiments carried out for 4 s, 20 s, 60 s, 300 s, and 600 s with fixed fluid viscosity and ultrasound power of 10 W and 30 W (Section 5.3.5 of Zeiger, 2012). The longest time of 10 minutes was selected as being the time when the size distribution changed very slowly for both values of ultrasound power. The model agreement with data was very good for all times (Figure 5.19 of Zeiger, 2012, not included here for brevity).

4 Conclusions

Population balance models for the breakage of aspirin crystals in dodecane and silicone oils due to ultrasonication are presented that relate breakage rate proportionally to ultrasonic intensity and exponentially to fluid viscosity. The resulting population balance models provide reasonable agreement with the experimental data over the ranges of applied power and solvent viscosity investigated, with nearly overlapping crystal size distributions for applied power between 10 and 40 W. A comparison of the crystal size distributions with experimental data provided more support for binary breakage events where the crystals break in half than for binary breakage events that produce uniformly distributed particle sizes. A 3-parameter model that generalized both equal-sized and uniformly distributed particle sizes did not produce statistically significant improvements in the model fit to the experimental particle size distributions. The dependency of the breakage rate on the particle mass was observed to be small for the binary equal-size breakage model. A thin flat shape of the aspirin crystals may explain why these crystals were well modeled by a binary equal-size breakage model.

This article describes the most advanced population balance model yet developed for describing ultrasound-induced breakage of crystals. Such models may have promise for the selection of ultrasonic conditions that best move a crystal size distribution towards a target distribution.

Acknowledgments

This work was supported by the National Science Foundation (DMR 09-06904) and the Process Systems Engineering Consortium.

References

Beck, J.V., Arnold, K.J., 1977. Parameter Estimation in Engineering and Science, Wiley, New York.

Broadbent, S.R., Callcott, T.G., 1956. A matrix analysis of processes involving particle assemblies, Philosophical Transactions of the Royal Society of London A, 249, 99–123.

Colussi, A.J., Hung, H.M., Hoffmann, M.R., 1999. Sonochemical degradation rates of volatile solutes, Journal of Physical Chemistry A, 103, 2696–2699.

Devarakonda, S., Evans, J.M.B.; Myerson, A.S., 2004. Impact of ultrasonic energy on the flow crystallization of dextrose monohydrate, Crystal Growth & Design, 4, 687–690.

Doktycz, S.J., Suslick, K.S., 1990. Interparticle collisions driven by ultrasound, Science, 247, 1067–1069.

Guo, Z.; Jones, A.G.; Li, N.; Germana, S., 2007. High-speed observation of the effects of ultrasound on liquid mixing and agglomerated crystal breakage processes, Powder Technology, 171, 146–153.

Lifshitz, D.A.; Williams, Jr., J.C.; Sturtevant, B.; Connors, B.A.; Evan, A.P.; McAteer, J.A., 1997. Quantitation of shock wave cavitation damage *in vitro*, Ultrasound in Medicine & Biology, 23, 461–471.

Raman, V., Abbas, A., 2008. Experimental investigations on ultrasound mediated particle breakage, Ultrasonics Sonochemistry, 15, 1, 55–64.

Raman, V., Abbas, A., Zhu, W., 2011. Particle grinding by high-intensity ultrasound: Kinetic modeling and identification of breakage mechanisms, AIChE Journal, 57, 8, 2025–2035.

Son, Y., Lim, M., Kim, J., 2009. Investigation of acoustic cavitation energy in a large-scale sonoreactor, Ultrasonics Sonochemistry, 16, 552–556.

Suslick, K.S., Didenko, Y., Fang, M.M., Hyeon, T., Kolbeck, K.J., McNamara III, W.B., Mdleleni, M.M., Wong, M., 1999. Acoustic cavitation and its chemical consequences, Philosophical Transactions of the Royal Society of London A, 357, 335–353.

Tan, H.S., Salman, A.D., Hounslow, M.J., 2004. Kinetics of fluidised bed melt granulation IV. Selecting the breakage model, Powder Technology, 143-144, 65–83.

Teipel, U., Leisinger, K., Mikonsaari, I., 2004. Comminution of crystalline material by ultrasonics, International Journal of Mineral Processing, 74, S183–S190.

Teipel, U., Mikonsaari, I., 2002. Size reduction of particulate energetic material, Propellants, Explosives, Pyrotechnics, 27, 168–174.

Wagterveld, R.M., Boels, L., Mayer, M.J., Witkamp, G.J., 2011. Visualization of acoustic cavitation effects on suspended calcite crystals, Ultrasonics Sonochemistry, 18, 216–225.

Zeiger, B.W., Suslick, K.S., 2011. Sonofragmentation of molecular crystals, Journal of the American Chemical Society, 133, 14530–14533.

Zeiger, B.W., 2012. *Bubbles and Crystals: Time Resolved Sonoluminescence, Sonocrystallization, and Sonofragmentation*. Ph.D. thesis, University of Illinois at Urbana-Champaign, 2012.

Figures

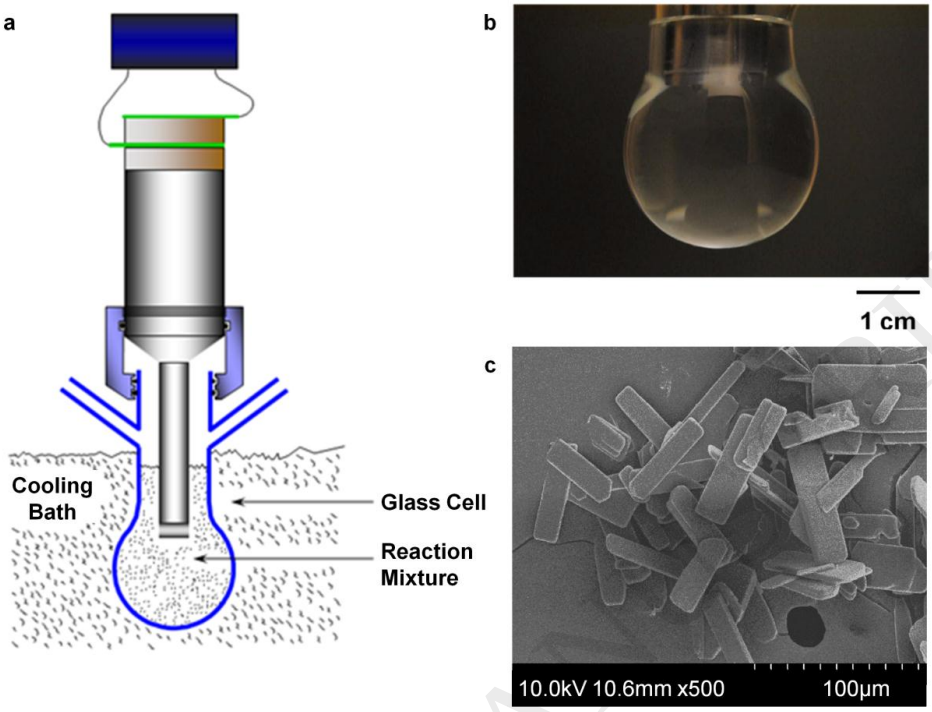

Figure 1: (a) Schematic of experimental setup for sonofragmentation experiments, with the 20 kHz ultrasonic horn shown in the middle with power supply at the top. (b) Photograph of glass cell within which fragmentation was induced. (c) SEM image of aspirin crystals synthesized in dodecane.

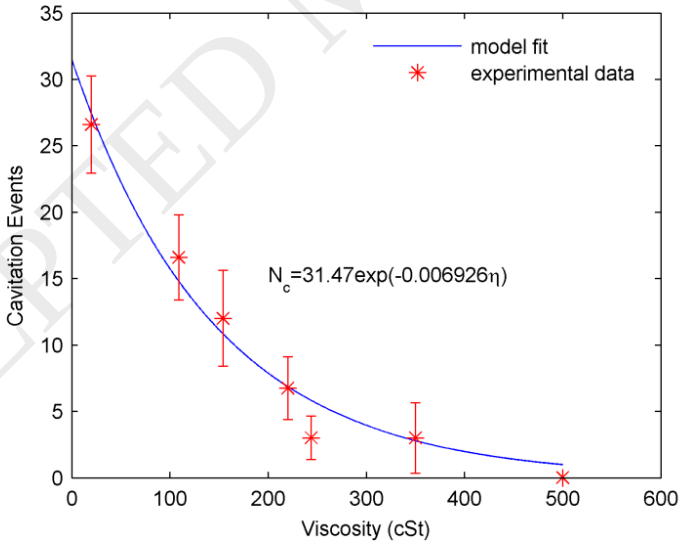

Figure 2: An exponential relationship was observed between the number of cavitation events and the liquid viscosity subjected to ultrasound. The experimental setup involved counting the number of holes generated by cavitation bubbles in a foil target in 40 mL of liquid at a specified distance from the probe tip for 30 seconds. A description of the laboratory system and experimental procedures to measure cavitation events is available elsewhere (Lifshitz et al., 1997), with the details of our specific experimental setup in Figure 5.14 and Section 5.3.4 of Zeiger (2012).

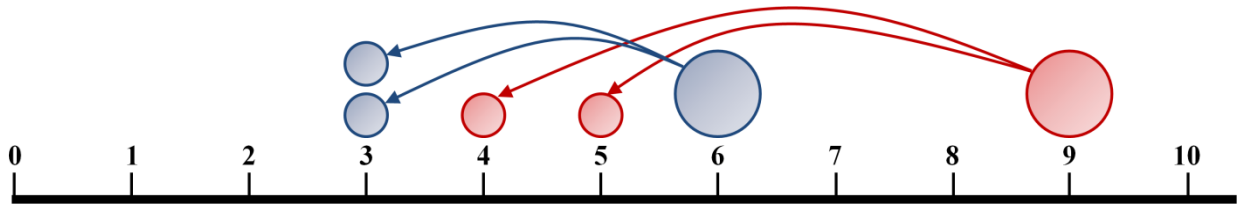

Figure 3: An equal binary breakage model with crystal masses restricted to integer values.

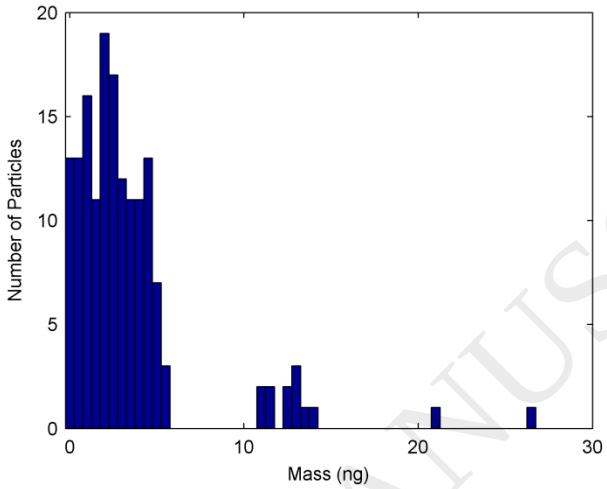

Figure 4: Histogram of crystal masses prior to sonication (159 representative particles shown).

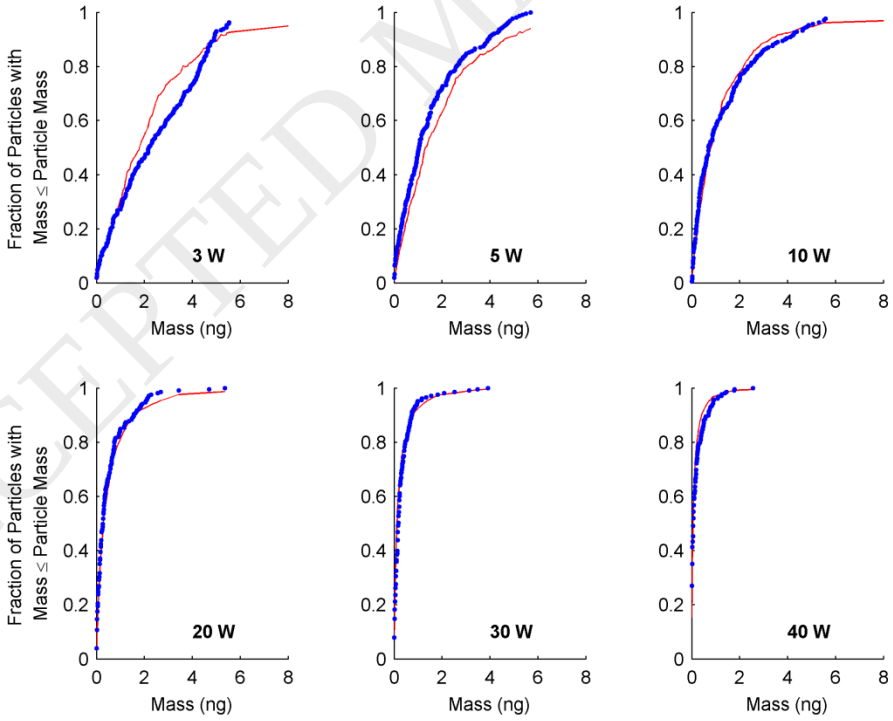

Figure 5: Cumulative mass distributions for the equal binary breakage model (7) with best-fit model parameters S_0 and q (red line) and experiments (blue dots) for variations in the ultrasonic power in the solvent dodecane (viscosity = 1.8 cSt). Due to finite sampling, fewer samples are observed near the tails of the mass distributions for 20, 30, and 40 W.

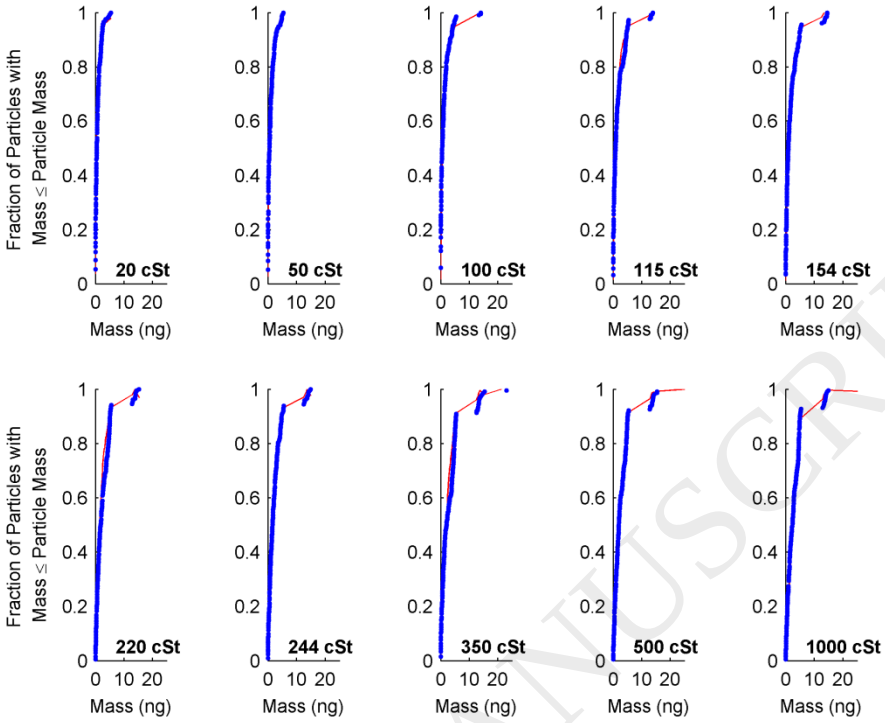

Figure 6: Cumulative mass distributions for the equal binary breakage model (7) with best-fit model parameters S_0 and q (—) and experiments (•) for variations in the liquid viscosity at an applied ultrasound power of 30 W. The gap between 6 and 10 ng observed in the mass distributions for large viscosities, which have limited breakage, corresponds to the gap reported in mass distribution before sonication (see Figure 4).

Table

Table 1: Coefficient of determinations (R^2) for the models with the optimal parameters for each breakage model and set of experiments. The equal-size breakage model provides nearly the highest R^2 while being simpler and having one less parameter than the normal breakage model.

Experiment	Breakage Model		
	Equal	Uniform	Normal
Power	0.951	0.820	0.955
Viscosity	0.964	0.873	0.964